Physico-chemical behaviors of human and bovine milk membrane extracts and their influence on gastric lipase adsorption

Claire Bourlieu, Wafa Mahdoueni, Gilles Paboeuf, Eric Gicquel, Olivia Ménard, Stéphane Pezennec, Said Bouhallab, Amélie Deglaire, Didier Dupont, Frederic Carriere, et al.

Title: Physico-chemical behaviors of human and bovine milk membrane extracts and their influence on gastric lipase adsorption

Running title: human and bovine milk membrane extracts interfacial behavior and their influence on gastric lipase adsorption

C. Bourlieu[1,26]*, W. Mahdoueni[1,2], G. Paboeuf[3,4], E. Gicquel [4], O. Ménard, S. Pezennec[1,2], S. Bouhallab[1,2], A. Deglaire[1,2], D. Dupont[1,2], F. Carrière[5], V. Vié[3,4]

[1]INRA, UMR 1253 STLO, France,
[2]Agrocampus Ouest UMR 1253 STLO, France;
[3] Univ Rennes, CNRS, IPR - UMR 6251, F-35042 Rennes, France
[4] Univ Rennes, CNRS, ScanMAT - UMS 2001, F-35042 Renne, France,
[5]CNRS, Aix-Marseille Université, UMR 7282 EIPL, France,
[6]INRA, UMR IATE, France.

Corresponding authors: *claire.bourlieu-lacanal@inra.fr, *veronique.vie@univ-rennes1.fr

Permanent address: UMR IATE 1208, 2 Place P. Viala, 34000 Montpellier, France

Abstract

Milk fat globule membrane conditions the reactivity and enzymatic susceptibility of milk lipids. The use of bovine membrane extracts to make infant formulas more biomimetic of human milk has been suggested recently. A comparison of the physico-chemical behavior of human and bovine milk membrane extracts and their interaction with gastric lipase is here undertaken using biophysical tools. Milk membrane extracts (70 % of polar lipids) were obtained either pooling of mature human milk (n=5) or bovine buttermilk. Human extract contained more anionic glycerophospholipids, less phosphatidylethanolamine and more unsaturated fatty acids (57 % *versus* 46 %) than bovine extract. Human extract presented a higher compressibility, with slower increase of surface pressure, than bovine extract. Micronic liquid condensed (LC) domains were evidenced in both extracts at 10 mN/m, but the evolution differs upon compression. Upon gastric lipase addition, an adsorption preference for liquid expanded phase (LE) was observed for both extracts. However, insertion was more homogeneous in terms of height level in human extract and impacted less its lipid lateral organization than in bovine extract. Both membrane extracts share close physico-chemical properties, however human membrane higher compressibility may favour gastric lipase insertion and higher interfacial reactivity in gastric conditions.

Keywords: milk fat globules, human milk membrane, bovine milk membrane, monolayer, AFM, gastric lipase adsorption, infant nutrition

Abbreviations: AFM, atomic force microscopy; BAM, Brewster angle microscopy; BMM, bovine milk membrane; DHA, docosahexaenoic acid; DPPC, dipalmitoylphosphatidylcholine; HGL, Human gastric lipase; HMM, human milk membrane; MFG, milk fat globule; MFGM, milk fat globule membrane; LE, liquid expanded; LC, liquid condensed; LO, liquid ordered; PC, Phosphatidylcholine; PE, phosphatidylethanolamine; PI, phosphatidylinositol; PL, polar lipids; PS,

Phosphatidylserine; rDGL, recombinant dog gastric lipase; SM, sphingomyelin, TAG, triacylglyceride.

1. Introduction

The main source of energy to support infant and children growth is lipid. Lipids are found in human milk under the specific form of fat globules (Figure 1), *i.e.* 4 µm lipoproteic assemblies based on an apolar core of triglycerides stabilized by a complex trilayered membrane [1, 2]. This lipid structure is shared among mammalian milks [3, 4]. The membrane contains proteins but is based predominantly on very diverse polar lipids (PL) [2, 5, 6]. This membrane called the milk fat globule membrane (MFGM) maintains the triglycerides dispersed in the aqueous phase of the milk but also conditions milk reactivity and its susceptibility to digestive lipases [1, 7-10].

Human milk remains a gold standard in infant nutrition [11, 12]. However, infant formulas are often administrated to infant when breast-feeding is not possible. These infant formulas are based on a blend of vegetable fat stabilized by protein and synthetic emulsifiers [13, 14]. Recent works in neonatal nutrition have suggested that developing more biomimetic infant formulas with a structure closer to human milk would lead to positive outcomes in terms of metabolism programming [15-18], immune competency and gut microbiome establishment [19]. BMM extracts found concentrated in some dairy coproducts such as buttermilk or butterserum seem reasonable substitute to human milk membrane (HMM) extracts [20-23]. Many physical properties of human MFG are inferred from data obtained on bovine MFG which have been paradoxically more characterized as lipoproteic assemblies than their human counterparts [3, 4, 24-26]. In short, the physico-chemical behavior of HMM extract has never been compared to the one of BMM.

HMM and BMM polar lipids are globally similar, gathering in both case hundreds of different molecules of PL (with variable polar heads and acyl chains), but differing on two

major points: HMM is expected to contain on average more SM than BMM; HMM acyl chains are on average more unsaturated than BMM [27-29]. In particular, HMM is rich in long chain polyunsaturated fatty acid of the omega 3 series such as docosahexaenoic acid (DHA) which is considered as essential for cerebral and visual development during the neonatal period. The capacity of bioconversion of linolenic acid and alpha-linolenic acid into long chain polyunsaturated fatty acids, is limited during neonatal period, inducing a dependence on the dietary intakes from human milk lipids [30].

Whatever the source of milk membrane, its lipid chemical complexity induces phase separation in the membranes. This phase separation leads to lateral heterogeneity in the membrane and to the appearance of domains in which molecular packing is higher [29, 31, 32]. These domains are generally enriched in PL containing more saturated and longer acyl chains, resulting in more ordered acyl chains and in liquid ordered (LO) organization. On the contrary, the liquid disordered phase is less compact and concentrates PL enriched in unsaturated and/or short chain fatty acids.

Lipid monolayer spread on Langmuir trough are an easy and relevant model to study biomembrane and intermolecular interactions [33]. Indeed, surface pressure induced by the molecular packing in the interface can be controlled while other direct characterization such as ellipsometry or imaging such as Brewster angle microscopy [34] can be conducted, to give information on the monolayer thickness and its morphology upon compression. In a previous study, [35] described lipid-lipid interaction and the formation of microdomains in monolayers of PL extracted from four bovine milk products (raw milk, raw cream, processed milk and processed cream) upon increasing temperature and lateral pressure. These authors combined the surface pressure measurements, epifluorescence microscopy on the interface of Langmuir trough and also conducted interfacial film transfers by the Langmuir-Blodgett method to image them by AFM.

The first digestive lipase interacting with human MFGM is gastric lipase [36-38]. Gastric lipase is a crucial player of lipid neonatal digestion as its secretion is high while the levels of secretion of pancreatic and bile are still limited [36, 39, 40]. In addition, gastric lipase initiates the lipolysis of MFGM, what is not done by pancreatic lipase [41]. GL is therefore able to interact with a biological substrates of high complexity but the mechanisms of interaction with human MFGM had not been described up to now.

It has been demonstrated using bovine MFGM monolayers to mimic the outer leaflet of the native membrane, that phase coexistence impacts gastric lipase adsorption [42, 43]. Gastric lipase got inserted in liquid expanded (LE) phase or at boundaries of liquid condensed (LC) phase in the bovine milk membrane (BMM) extract. Its insertion was mediated by hydrophobic and electrostatic interactions. Gastric lipase adhered or got inserted at several height levels depending on the local packing of the lipids around the gastric lipase molecules. These different height levels could correspond to various levels of interactions of the lipase with membrane PL. In addition, AFM topographic images of the lipases in this complex membrane system indicated clusters or alignments of molecules suggesting cooperation in lipase insertion.

Interfacial behavior of HMM extracts has never been investigated nor its consequences on interactions between this extract and gastric lipase. It is thus the objective of our study, to characterize the physicochemical behavior of monolayer of HMM extracts in comparison with BMM and their interaction with gastric lipase. More precisely, the way surface pressure, compressibility, local surface charge and phase coexistence modulates gastric lipase interaction with HMM extracts in comparison with BMM extracts will be analyzed.

2. Experimental

2.1. Materials

Unless otherwise stated, chemicals were from commercial origin (Sigma-Adrich, Saint-Quentin Fallavier, France).

2.2 Enzyme

Recombinant dog gastric lipase (rDGL) was produced by Meristem Therapeutics (Clermont-Ferrand, France) in transgenic maize and purified as described previously [44]. rDGL stock solution was prepared at a concentration of 1.1 mg mL−1 in 10 mM MES (2-(N-morpholino)ethanesulfonic acid) (pH 6.0) containing 150 mM NaCl and was further diluted in sodium acetate buffer (10 mM) at pH 5 (100 mM NaCl, 20 mM CaCl2) prior to monolayer experiments as described previously [7, 45].

2.2. Preparation of membrane extracts

Monolayers were prepared from polar lipids extracted from pooled raw mature human milks or bovine milk buttermilks or and used as a model system to mimic each type of milk fat globule membrane.

2.2.1. Human milk membrane extract

Mature human milk was obtained from Rennes Lactarium under ethical agreement n°13-12. Milk was given by five anonymous donors on average at 11 weeks after birth (collection period spans over 6-14 weeks). Milks were pooled using similar volume of raw milks at 4°C. After pooling milk was stored at -20°C. Macronutrients composition was determined using calibrated infrared analyzer (Miris Beledico, Villeurbanne, France). The pool was based on 2.7±0.2% lipids, 1.1±0.1% proteins and 8.0±0.2% carbohydrates. Total lipids were obtained by Folch extraction. Membrane lipids were then further extracted using acetonic extraction.

2.2.2. Bovine milk membrane extract

A bovine buttermilk powder was supplied by LACTALIS (Retiers, France). Milk polar lipid raw fraction (MPL) was obtained from this buttermilk powder by Folch extraction followed by further purification using acetonic extraction. The resultant extract contained residual

neutral lipids (31.4 % TAG, 69.4 % PL).

2.3. Chemical characterization of membrane extracts

The PL classes and total fatty acids of these two extracts were characterized by HPLC and GC following methodologies previously published [46].

2.4. Biophysical characterization of the extracts

2.4.1 Ellipsometry and surface tension measurements at the air/liquid interface

A computer-controlled and user-programmable Langmuir trough of 100 cm^2 (Nima Technology, Cambridge, UK) equipped with two movable barriers was used for the pressure–area isotherm recording. The surface pressure was measured with a filter paper held by a Wilhelmy balance connected to a microelectronic feedback system ($\pi=\gamma 0-\gamma$, where $\gamma 0$ and γ are the surface tension values in the absence and presence of lipids at the air/liquid interface, respectively). The surface pressure (π) and the ellipsometric angle (Δ) were recorded simultaneously as a function of the specific area (Asp, $mg.m^{-2}$). Values of π were recorded every 4 s with a precision of ± 0.2 $mN.m^{-1}$. Ellipsometric measurements were carried out with a home-made automated ellipsometer in a "null ellipsometer" configuration [47]. The laser beam probed a surface of 1 mm^2 and a depth in the order of 1 µm and gives insight on the film thickness. Values of Δ were recorded every 4 s with a precision of ±0.5°. Before starting the experiment, the trough was cleaned with chloroform and Millipore water. It was then filled up with 50 mL of the subphase (10 mM sodium acetate buffer (pH 5) containing 100 mM NaCl and 20 mM $CaCl_2$) and the air/liquid interface was cleaned of impurities by repeated aspiration and verification of the (π–A and Δ-A) isotherms each time. A good baseline in the isotherms indicated the cleanliness of the interface. The lipid solution ($10mg.mL^{-1}$) in chloroform/methanol (2:1) were spread at the air/liquid interface using a high precision Hamilton microsyringe. After evaporation of the solvent (10 min), the π–Asp and Δ-

Asp isotherm of lipid monolayer was measured by compressing the barriers at the rate of 5 $cm^2.min^{-1}$. The temperature was kept constant at 21.0±0.5 °C. Each experiment was repeated at least two times.

Monolayer compressibility was obtained from isotherm as indicated by [48] using equation 1 and considering an average molecular weight of 752 $g.mol^{-1}$ for HMM extract and 743 $g.mol^{-1}$ for BMM extract determined based on HPLC analysis:

$$C_s = -\frac{1}{A} \times \frac{dA}{d\pi} \qquad (1)$$

*where A is the area per molecule at the indicated surface pressure and π is the corresponding surface pressure. For ease of comparison with previously published data, we represented the reciprocal of isothermal compressibility i.e., (C_s^{-1})*as a function of *average cross-sectional molecular (Figure 2 C and D). Such mode of expression facilitates comparison the bulk elastic moduli of area compressibility measurements made in bilayer systems. C_s^{-1} values were obtained at equally spaced surface pressures (0.2 $mN.m^{-1}$ intervals) over the range of 1 to above collapse pressure (50-60 $mN.m^{-1}$).*

2.4.2 Brewster angle microscopy

Morphological features of monolayers during compression were observed using Brewster angle microscopy. Indeed, this technique is useful to follow the dynamic events during the compression of monolayers in a Langmuir trough. Brewster angle microscopy was preferred to epifluorecence microscopy (equivalent lateral resolution) as it does not require any dye that could interfere with the monolayer physical behavior. An ellipsometer EP3 (Nanofilm, Berlin, Germany) with a polarized incident laser (λ = 532 nm) was used with a 10× objective in a Brewster angle configuration (angle of incidence was 53.1°)[49]. The lipids were spread successively at the interface to increase step by step the surface pressure to the target surface pressure. After surface pressure stabilization the images were recorded. The images represented a 450 µm × 390 µm surface. Different zones of each sample were evaluated; the images here shown are representative of the whole samples.

2.4.3 Atomic force microscopy

AFM imaging was conducted either on Langmuir-Blodgett transferred films exposed in the

air or in liquid mode on Langmuir-Schaefer transferred films. For the first type of observations, the film was transferred onto a freshly-cleaved mica plate at a constant surface pressure and at a very low speed (0.5 $mm.min^{-1}$). The observations were performed with an atomic force microscope (Molecular Imaging, Pico+, Plus, Scientec, France) in contact mode in air (20°C) with standard silicon cantilevers (spring constant of 0.06 or 0.12 $N.m^{-1}$, SNL, Bruker, France). The scan rate was 1 Hz. The force was adjusted to a minimum during all the scans. To verify the integrity of the sample after the different scans and zooms, the same zone was imaged at the end of the analysis. The scanner size was 100×100 μm^2. Presented images are representative of at least duplicated experiments. The images were processed (flattened using 2nd level of polynomial processing implemented on Picoscan 5.3 software (Molecular Imaging Corporation, San Diego, USA). The differences of height between LC and LE phases (d_{LC-LE}) were assessed by random measurements (N=20 on 5×5 μm^2 image) on cross-sections of the image using Gwyddion.

With regards to the second type of imaging on Langmuir-Schaefer transferred films, several steps of preparations of the sample were required. First hydrophobic mica was hydrophobized by transferring by Langmuir-Blodgett method a HMM or BMM monolayer onto freshly cleaved mica disc at high surface pressure (35 $mN.m^{-1}$). After two days of dehydration, the coated mica could be used. The sealed (bottom side) AFM Teflon chamber was placed at the bottom of the trough. At the end of the lipase absorption kinetic (~4 hours), the interfacial film was collected by lowering horizontally the hydrophobic mica disc at very low speed (0.5 mm/min) using the dipper of Nima technology (England). After contact with the film, the sample was maintained blocked on the sealed chamber. Then all system was reverted and the chamber was placed on the AFM (Molecular Imaging, Pico+, Plus, Scientec, France). The sample was maintained hydrated all the time. The liquid level of the chamber could be readjusted with 10 mM sodium acetate buffer (pH 5) containing 100 mM NaCl and 20 mM

$CaCl_2$. Imaging was carried out in contact mode at room temperature as described before for Langmuir-Blodgett transferred films.

2.5. Characterization of enzyme/extract interaction at air/water interface

The monolayer was performed by spreading lipids from the stock solution (10 $mg.mL^{-1}$ in chloroform) over the clean air/liquid interface of the Langmuir trough using a high precision Hamilton microsyringe until an initial surface pressure of 20 ± 0.5 $mN.m^{-1}$ was reached. rDGL was further injected into the sub-phase of the trough at a 40 nM final concentration as previously described [7]. The surface pressure was continuously recorded. An increase appeared when the protein insertion to onto the lipid monolayer occurred and the equilibrium surface pressure was reached at the end of the kinetics. The Langmuir-Blodgett transfer was then performed and analyzed by AFM.

2.6. Statistics

All results to be presented as significantly different between the two extracts were tested by T-test using R software (R.2.13.0, http://cran.r-project.org). Differences between groups were declared significant at $p<0.05$ or $p<0.01$.

3. Results

3.1. Chemical composition of the membrane extracts impacts on its morphology upon compression

HMM and BMM extracts share similar PL composition (Table 1) with a profile dominated by SM and PC, though with an inversion: SM is predominant in HMM whereas it is PC in BMM. Three glycerophospholipids (PS, PI, PE) are also present in both extracts. In HMM anionic glyceroPL (PS and PI) are more numerous than in BMM. When looking now at the

corresponding acyl chain lengths esterified in the extracts, it is very broad in both extracts although with more unsaturated FA in HMM (57.1±0.1%) than in BMM (46.8±0.0%).

This heterogeneity results in lateral segregation in physiologic conditions which can be approached in monolayers by progressive compression in Langmuir trough, but also using BAM which allows the dynamic characterization of the monolayer at various surface pressures. Surface pressure / specific area (π-Asp) and ellipsometric angle / surface pressure (Δ-π) isotherms are shown in figure 2A and 2B respectively. Corresponding Surface pressure and calculated Surface compressional moduli/ Mean molecula area (π and C_s^{-1}-A) are presented in figure 2D and 2E respectively for HMM and BMM monolayers. The monolayers of HMM and BMM were compressed up to the pressure collapse at 20°C (Figure 2A). The two extracts presented a surface pressure increase upon compression beginning with a plateau typical of gas/liquid expended phase coexistence observed at a surface pressure of 0 $mN.m^{-1}$. This plateau was followed by an increase up to a kink around 44 $mN.m^{-1}$for both extracts corresponding to the collapse [50]. The surface pressure provides information on the lateral interaction between lipids upon compression. The ellipsometric angle (Δ) is both proportional to the reflective index and to the thickness of the lipid film. The reflective index can be considered constant during compression permitting to consider Δ as a function of the film thickness.

No surface characterization data has been produced up to now on HMM. When comparing BMM and HMM, the first observation and difference between them, is the position of the lift-off point (where $\pi \neq 0$ at this time the molecules begin to interact together. For HMM, the increase of surface pressure begins at the 0.99±0.05 $m^2.mg^{-1}$while for the BMM the value is of 0.76±0.10 $m^2.mg^{-1}$. This difference is associated to the 1° of variation in the film thickness which is lower for HMM (5± 0.1°) than BMM (6±0.1°). This difference could result from the presence of long unsaturated acyl chains which increased the chain

flexibility favoring lateral chain/chain interactions even at very low surface concentration. At this stage, the lipid packing increased the surface pressure and the ellipsometric angle. At 10 $mN.m^{-1}$ the ellipsometric angle of the HMM increases faster than for BMM, while the increase of surface pressure with respect to the specific area is slower. Moreover, around 18 $mN.m^{-1}$, a slight plateau in the evolution of surface pressure, with respect to the specific area, appeared up to 25 $mN.m^{-1}$. This phenomenon was not observed for the BMM and can be attributed to the high amount of long unsaturated acyl chains. Finally, the collapse values for both extracts were similar 44.6 and 43.7 $mN.m^{-1}$ for BMM and HMM respectively. However, the specific area values were very different with a variation close to 0.18 $m^2.mg^{-1}$, and the ellipsometric angle values at collapse differ by 4.5°.

When the lipid films were compressed beyond the collapse value, the surface pressure remained stable whereas ellipsometric angle evolutions differed between the two extracts: the further increase of angle for BMM suggested stable multilayer formations whereas the further decrease of angle observed for HMM indicated loss of interfacial matter.

Surface compressional moduli/ Mean molecula area (C_s^{-1}-A) curves displayed in Figure 2D and 2E give detailed information about the films structure and their lipid components interactions. It is expected that C_s^{-1} goes through a maximum well below collapse pressure and then decreases at higher surface pressure. HHM films compressional moduli (Figure 2C) present three maxima below collapse pressure at almost same values: C_s^{-1}=37.9 $mN.m^{-1}$ (π=11.7 $mN.m^{-1}$, A=80.6 $Å^2.molecule^{-1}$), C_s^{-1}=36.2 $mN.m^{-1}$ (π=30.6 $mN.m^{-1}$, A=40.1 $Å^2.molecule^{-1}$), C_s^{-1}=36.3 $mN.m^{-1}$ (π=39.8 $mN.m^{-1}$, A=29.2 $Å^2.molecule^{-1}$). HMM also presented a mimimum for π=24.4 $mN.m^{-1}$ with C_s^{-1}=20.7 $mN.m^{-1}$ and A=50.6 $Å^2.molecule^{-1}$. In comparison, BMM films compressional moduli (Figure 2D) was much higher below collapse point and presented a steady increase up to collapse. Maximum was 10 times higher than HMM C_s^{-1} maxima and reached 377.4 $mN.m^{-1}$ (π=43.0 $mN.m^{-1}$, A=50.6 $Å^2.molecule^{-1}$).

Comparison of compressional moduli indicated a much higher compressibility of HMM films in comparison to BMM films and a range of low C_s^{-1} and thus high compressibility for pressure ranging between 17.3 to 24.4 mN.m^{-1} in HMM films.

This films characterization was strengthened by BAM observations which are summarized in Figure 3 and allowed the characterization of more transient phenomena in the morphologies of the films upon compression at low resolution. Indeed, domains appeared at very low surface pressure as a gas/liquid expended phase coexistence (dark gaseous phase and light liquid expanded phase) is observed, this phase is called 2D foam phase. Then at 10 mN.m^{-1}, the images for both extracts became homogeneous in gray scale even if in BMM some lighter spots than the background can be detected. At 20 mN.m^{-1}, some domains were clearly observed in the BMM film resulting of LE/LC phase coexistence while the HMM film remained homogeneous. The LC phase is formed by saturated chains of lipids (C14:0; C16:0; C18:0), SM is organized in this phase in monolayer at the surface pressure around 18 mN.m^{-1} [51] and is present in both extracts. This phase coexistence didn't appear as a plateau in the BMM isotherms like in pure saturated lipid because it was hidden in the global surface pressure increase due to the presence of unsaturated lipids [52]. In contrast at 30 mN.m^{-1}, the background is lighter for HMM than BMM. Moreover white spots appeared in HMM while the images became homogeneous for BMM. This is in agreement with the increase of thickness of HMM observed in (Δ-π) curve. At 40±1 and 44±1 mN.m^{-1}, in both extracts, bright spots were present, resulting from 3D structure formation.

In order to investigate further the film structures, atomic force microscopy was performed to obtain topographic images with a nanometer resolution. Figure 4 and Figure 5 showed the AFM images taken at different surface pressure for the HMM and BMM membrane lipid extracts respectively.

At 10 mN.m^{-1}, the AFM images revealed LC domains in both extracts, nevertheless the

diameters were higher for BMM (~4µm) than HMM (~1µm) explaining the possibility to be observed by BAM only for BMM. When increasing the surface pressure, the domains present in HMM film grew laterally and slightly while keeping a circular shape, the mean diameter was around 4 µm. On the contrary in the BMM, and in agreement with previous studies [35], domain growth is made by association of nanodomains resulting in flower shapes having diameters around 20 µm. The two growth processes reveal difference in line tensions between the two extracts: despite increase in surface pressure, line tension in BMM remains high, allowing domain association but no fusion. On the contrary, the energy per interface line between LE and LC is lower in HMM then in BMM allowing direct domain growth. Furthermore, the shape and the repartition of LC domains are induced by a competition between line tension and long range electrostatic interaction (or dipolar repulsion)[53]. In HMM, the individual domain growth associated to the circular shape means a minimization of line energy and the presence of long range repulsive interactions between domains. The charged lipid composition differs between both extract as mentioned above with % more of PS and PI in HMM. The surface pressure increase beyond the collapse favors interfacial 3D structures either under the form of multilayers or of unstructured objects. Here again, both extracts display two distinct behaviors as shown in BAM and AFM images correlated with the Δ evolution. For the HMM, apparition of numerous very bright spots at 40 $mN.m^{-1}$ in BAM images revealed 3D structure formation observed also in AFM images, the Δ increased continuously up to the collapse value 43.7 $mN.m^{-1}$ from which a decrease occurred suggesting loss of matter at the interface in the range of 4 $mN.m^{-1}$. Then, PI molecules could locally destabilize the interface by strong head-group interactions between inositol and provoke the expulsion of some instable lipid aggregates at these pressures moreover the negative surface density (23% of negatively charge lipids) could prevent interfacial trilayers or multilayers. Then, the surface pressure and the thickness follow to increase during few $mN.m^{-1}$before to

fall again. In contrast, at 40 $mN.m^{-1}$, the BMM did not present interfacial 3D structures and after the collapse surface pressure the Δ strongly increased suggesting the multilayer formation as confirmed by the topographic images at 51 $mN.m^{-1}$. These multilayers were previously observed using phospholipids as dimyristoylphos-phatidylcholine (DMPC) [54] or bolalipids [55] highlighting an ability of this lipid mixture essentially composed of PC to form multilamellar structures. Moreover, the presence of PE lipid in the mixture can initiate the multilamellar structure formation. Due to the balance between the head-group/acyl chain volume, PE is known to induce curvature in bilayers or monolayers [56]. To conclude, insaturations and charges modified drastically the 2D behavior of the HMM compared to the BMM inducing the ability to be compress at the surface pressures between 18 and 27 $mN.m^{-1}$. Then the subsequent question was what is the impact of such difference of compressibility on lipase absorption.

3.2. Adsorption of lipase into the milk membrane extracts at 20 mN

Following lipase injection, variation of both ellipsometric angle and surface pressure were recorded and can be related with an influx of lipase triggering reorganization in the monolayer followed by the relaxation of the film (Supplementary data Figure 1). In BMM, lipase injection triggered an increase in surface pressure of 2.1±0.2 $mN.m^{-1}$ and of 3.4±1.4° of delta (250 minutes after injection). In comparison, lipase adsorption induced a decrease in surface pressure -3.2±0.6 $mN.m^{-1}$ but a concomitant very high increase in delta (13,2±0.0°) in HMM. AFM observations of the Langmuir-Blodgett lipid films in the absence or after the injection of rDGL in the subphase were conducted to investigate the distribution of rDGL at the nanoscale level (Figure 6). Before the injection of lipase, both extracts displayed typical phase separation with LC (lighter zones) and LE (background) domains of variable shapes and size. In HMM, LC phase was present under the form of ovoid to bean-like domains (circularity

parameter=0.80) with average size of 0.6 µm^2 covering 13.6 % of the surface (Table 2). In BMM, LC phase was more important and heterogeneous. Indeed, this phase was dispersed as either large ovoid domains (circularity parameter=0.79) presenting an average size of 3.3 µm^2 and covering 24 % of surface, or found under the form of very small domains of 0.02 µm^2 on average covering 2.9 % of surface. Difference of height between LC and LE domains averaged 1.5 nm in both extracts.

The addition of rDGL clearly modified the film in both extracts: rDGL injection triggered the appearance of smaller domains as dispersed small "grains". These grains appeared in LE phase only in both extracts. These grains were more aligned in BMM then in HMM. The appearance of these grains also induced the smoothing of the edge of BMM LC domains whereas HMM LC domains' edge were already smooth in systems without rDGL. Image analysis indicated that these nanodomains covered 26.1 % and 29.5 % of surface in 20×20 image respectively in HHM and BMM films. Their average size was of 0.02 and 0.03 µm^2 respectively. Difference of height between LC and LE domains was not affected by rDGL injection. In BMM, these grains presented variable heights but can be subdivided into three main groups: less frequent but sharp peaks with height>5 nm, peaks ranging between 3 and 4 nm, *i.e.* just above the LC height, and eventually peaks ranging between 0-2 nm. In HMM, grains appearing after the adsorption of rDGL were more homogeneous in height, all around 3-4 nm. Langmuir-Schaefer transfers were also performed and imaged in liquid by AFM for both extracts (Figure 7). The presence of protein is clearly identified by bright spots recovering unevenly the surface. Successive scans (20µm×20µm for HMM and 1µm×1µm for BMM) removed the adsorbed proteins revealing intact lipid domains (without proteins) and protein inserted in the rest of the films.

4. Discussion

4.1. HMM film isotherm indicates higher compressibility than BMM

First of all, the BMM isotherms are in accordance with the literature [35, 57]. Slight differences can appear due to the buffer used; in fact, the presence of ions can modulate the space of the lipid head-groups. The type of extraction used, which may slightly modulate composition of the extract in terms of PL/TAG ratio or fatty acids profile in the extract, can also impact the isotherm. With regards to HMM, it is the first interfacial characterization of such extract despite its biological importance. The results of isotherm upon compression underlined the higher compressibility of the HMM film compared to the BMM film. This ability to be compressed is associated to an increase of the thickness at high surface pressure. It has been shown in DPPC liposomes that the addition of unsaturated fatty acids such as DHA and eicosapentaenoic acid induced a broadening and a shift of the Tm values of DPPC to lower temperatures (from 41 to 36°C). This resulted in more disordering and fluidity in DPPC bilayers [58]. This lowering of melting point is explained by reduction of intra and intermolecular Van Der Waal's interactions due to membrane packing modification related to the accommodation of multiple double bonds. More generally, the higher content in DHA in HMM (0.8%) is a key factors that enhances the fluidity, elastic compressibility and protein activity in the film [59]. The higher compressibility of HMM could also be linked to the fact that upon compression DHA can squeeze out from the monolayer [60]. DHA content in membrane can also impact interactions with proteins and membrane protein functions through three main mechanisms, enhancement of curvature stress, modification of membrane thickness and increase in acyl chain packing free volume [61].

4.2. HMM and BMM slight differences in PL headgroups contribute to different interfacial reactivity

The headgroups of PL differed between HMM and BMM with less PE and more PS in HMM than in BMM. These differences are in agreement with previously reported data on

both types of extracts [23, 25, 62]. Higher content in SM was also expected in HMM, similar trend is observed but difference is not significant in our work. Predicting the phase behavior of such complex system is extremely difficult. Similarly, disentangling the respective influence of parameters in complex biomembranes is a challenge. In our previous work however, we established that the addition of a small amount of negative charge using phosphatidylserine (10%) increased rDGL adsorption [7]. In addition, rDGL surface potential modelling at pH 5 indicated positive charges on the edges of an apolar ring surrounding the lipase active site and negative charge opposite the entrance of the active site. Thus, we can here speculate that the higher content in anionic phospholipid in HMM (PI and PS) may facilitate rDGL orientation and adsorption through electrostatic interactions. Since rDGL share high structural homology with HGL notably in charge distribution, such contributions of electrostatic interactions to HGL adsorption into HMM should also be observed in physiological conditions of digestion in human [44, 63]. It would also be of interest to question further this complementary of charge between milk fat globule membrane within different mammalian species and preduodenal lipases. BMM and HMM also contain small amounts of ceramides [23], which are characterized by small polar heads and can affect the membrane curvature and tend to segregate forming highly ordered domains [64]. Their presence could be beneficial factors, limiting packing and enhancing to a certains degree, lipases adsorption.

4.3. Liquid phase coexistence impacts on gastric lipase distribution in both extracts

In both extracts, the chemical complexity of membrane constituents in terms of acyl chains and headgroups resulted in phase coexistence. In agreement with what had been observed in BMM, we established that the coexistence of LC/LE phase in human milk membrane was an important driver of in gastric lipase distribution, since the lipase adsorbs

only in expanded phase. In such phase, lower molecular packing, probably enhanced by the presence of PUFA, favour gastric lipase adsorption. Similarly, AFM studies in supported monolayers or bilayers had indicated preferential adsorption of lipases and phospholipases at the edge of defects characterized by lower molecular packing [65-68]. Pancreatic lipase and colipase have been shown to selectively get adsorbed in LE regions in dipalmitoylphosphatidylcholine (DPPC) monolayers at the air−water interface in the presence of bile salts. In such systems bile salt progressively adsorbed onto DPPC interface, inducing the fractionation of LC domains and more edges with LE phase where lipase could adsorb [69].

4.4. Depth of penetration of gastric lipase within monolayer is more homogeneous in HMM than in BMM extracts

In HMM monolayers, the levels of insertion of rDGL with peaks of homogeneous height around 3-4 nm correspond to levels of insertion of the lipase of 1-2 nm which correspond to an insertion of the lipase in its active form [45, 65]. The surface covered by the peaks linked to rDGL presence underneath or adsorbed into the film are very similar in both extracts but the insertion of rDGL in BMM is less homogeneous in terms of depth of penetration. In this case the three levels of insertion of rDGL has been previously described: lower peaks may correspond to denaturated lipase totally inserted in the monolayer and acting as sacrifizing agent to lower tension and ease the insertion of other molecules; the intermediate level would coincide to the active form of the lipase as found in HMM; the highest peaks would correspond to lipase not inserted at all but only adsorbed underneath the monolayer.

Several physico-chemical attributes of HMM (high content in PUFA, presence of DHA, presence of anionic phospholipid, coexistence of LC/LE phase) tend to result in effective adsorption of rDGL in its active forms into these films. This membrane attributes are probably

involved in efficient prehydrolysis of the human milk fat globules. We can even speculate that the particular composition of HMM is even more favourable than the composition of BMM for the action of gastric lipase. The step of prehydrolysis of human milk fat globules by bile salt stimulated lipase but also by gastric lipase is a key step in the digestive fate of this substrate. Indeed, this step enhances the further action of pancreatic triglyceride lipase but also of the carboxyl ester lipase [41, 70]. Recent studies in animal model (neonatal mice) have indicated that the predigestion of fat triglyceride in formula may help preventing necrotisis enterocolitis in preterms [71]. Hence, fast prelipolysis of HM fat can be an important biological feature probably also favored by HMM globule membrane composition and high interfacial compressibility.

5. Conclusions

The membrane of milk fat globules conditions their reactivity at interfaces and interaction with digestive lipases. Here, we present a comparative physico-chemical characterization of human *versus* bovine milk membrane extracts which pointed out several similarities in terms of global chemical composition and coexistence of phases in the two extracts. Behavior in compression of film monolayers indicated an higher compressibility of HMM probably linked to its higher content in PUFA and notably in DHA. In both extract gastric lipase (rDGL) got inserted in liquid expanded phase with high surface coverage and impacted on lipid phase lateral organization. In HMM however, adsorption of rDGL was mainly observed at a depth of penetration compatible with the active form of the lipase and seems thus more effective. The presence of less tight molecular packing and more anionic phospholipids were positive parameters in HMM possibly favoring lipase adsorption.

Acknowledgements. The BIOMIF platform ('Biological Molecules at fluid interfaces, IPR, Rennes, France) is acknowledged for allowing all the biophysical characterization of samples presented in this article.

Funding. This work was supported by INRA CEPIA department.

Contributors.
The contributions of each author to the work is as follows:
- conception of the work: C. Bourlieu, V. Vié and C. Carrière
- collection of data: W. Mahdoueni, G. Paboeuf, E. Gicquel, O. Ménard
- analysis of data: W. Mahdoueni, G. Paboeuf, S. Pezennec, S. Bouhallab, A. Deglaire, D. Dupont, C. Bourlieu, V. Vié, C. Carrière
- writing of manuscript: C. Bourlieu, V. Vié and C. Carrière
All authors have approved the final article.

References

1. Bourlieu, C. and M.C. Michalski, **Structure–function relationship of the milk fat globule**. Current Opinion in Clinical Nutrition & Metabolic Care,18 (2015).
2. Gallier, S., A. Laubscher, and R. Jimenez-Flores, *Chapter 4 - The Milk Fat Globule Membrane: Structure, Methodology for its Study, and Functionality*, in *Food Structures, Digestion and Health*, M. Boland, M. Golding, and H. Singh, Editors. 2014, Academic Press: San Diego. p. 107-142.
3. Bourlieu, C., et al., **Towards infant formula biomimetic of human milk structure and digestive behaviour**, in *OCL*, 24 (2017).
4. Michalski, M.-C., *Lipids and milk fat globules properties in human milk*, in *Handbook of dietary and nutritionnel aspects of breast milk*, S. Zibadi, R.R. Watson, and V.R. Prudy, Editors. 2013, Wagueningen Academic Pusblishers: Wagueningen. p. 310-329.
5. Fong, B.Y., C.S. Norris, and A.K.H. MacGibbon, **Protein and lipid composition of bovine milk-fat-globule membrane**. International Dairy Journal,17 (2007), pp. 275-288.
6. Jensen, R.G., **The Composition of Bovine Milk Lipids: January 1995 to December 2000**. Journal of Dairy Science,85 (2002), pp. 295-350.
7. Bourlieu, C., et al., **Adsorption of gastric lipase onto multicomponent model lipid monolayers with phase separation**. Colloids and Surfaces B: Biointerfaces,143 (2016), pp. 97-106.
8. Gallier, S., et al., **In vivo digestion of bovine milk fat globules: Effect of processing and interfacial structural changes. I. Gastric digestion**. Food Chemistry,141 (2013), pp. 3273-3281.
9. Gallier, S., et al., **In vivo digestion of bovine milk fat globules: Effect of processing and interfacial structural changes. II. Upper digestive tract digestion**. Food Chemistry,141 (2013), pp. 3215-3223.
10. Lopez, C., C. Cauty, and F. Guyomarch, **Organization of lipids in milks, infant milk formulas and various dairy products: role of technological processes and potential impacts**. Dairy Science & Technology,95 (2015), pp. 863-893.

11. Le Huërou-Luron, I., S. Blat, and G. Boudry, **Breast- v formula feeding: impacts on the digestive tract and immediate and long-term health effects**, in *Nutrition Research Reviews*. 2010. p. 23-36.
12. Victora, C.G., et al., **Breastfeeding in the 21st century: epidemiology, mechanisms, and lifelong effect**, in *The Lancet*. 2016. p. 475-490.
13. Bourlieu, C., et al., **Infant formula interface and fat source impact on neonatal digestion and gut microbiota**. European Journal of Lipid Science and Technology,117 (2015), pp. 1500-1512.
14. Hageman, J.H.J., et al., **Comparison of bovine milk fat and vegetable fat for infant formula: Implications for infant health**. International Dairy Journal,92 (2019), pp. 37-49.
15. Baars, A., et al., **Milk fat globule membrane coating of large lipid droplets in the diet of young mice prevents body fat accumulation in adulthood**. Br J Nutr,115 (2016), pp. 1930-1937.
16. Oosting, A., et al., **A More Breast Milk-Like Infant Formula Reduces Excessive Body Fat Accumulation in Adult Mice**. Pediatr Res,70 (2011), pp. 837-837.
17. Oosting, A., et al., **Effect of dietary lipid structure in early postnatal life on mouse adipose tissue development and function in adulthood**. British Journal of Nutrition,111 (2014), pp. 215-226.
18. Oosting, A., et al., **Size and phospholipid coating of lipid droplets in the diet of young mice modify body fat accumulation in adulthood**. Pediatr Res,72 (2012), pp. 362-369.
19. Le Huerou-Luron, I., et al., **A mixture of milk and vegetable lipids in infant formula improves gut digestion, physiology and microbiota in neonatal piglets.** European Journal of Nutrition,(2016).
20. Conway, V., S.F. Gauthier, and Y. Pouliot, **Buttermilk: Much more than a source of milk phospholipids**. Animal Frontiers,4 (2014), pp. 44-51.
21. Gallier, S., et al., **A novel infant milk formula concept: Mimicking the human milk fat globule structure**. Colloids and Surfaces B: Biointerfaces,136 (2015), pp. 329-339.
22. Gassi, J.Y., et al., **Preparation and characterisation of a milk polar lipids enriched ingredient from fresh industrial liquid butter serum: Combination of physico-chemical modifications and technological treatments**. International Dairy Journal,52 (2016), pp. 26-34.
23. Bourlieu, C., et al., **Polar lipid composition of bioactive dairy co-products buttermilk and butterserum: Emphasis on sphingolipid and ceramide isoforms**. Food Chemistry,240 (2018), pp. 67-74.
24. Michalski, M.-C., et al., **Size distribution of fat globules in Human colostrum, breast milk and infant formula**. Journal of Dairy Science,88 (2005), pp. 1927-1940.
25. Zou, X., et al., **Lipid Composition Analysis of Milk Fats from Different Mammalian Species: Potential for Use as Human Milk Fat Substitutes**, in *Journal of Agricultural and Food Chemistry*. 2013, American Chemical Society. p. 7070-7080.
26. Zou, X.Q., et al., **Human Milk Fat Globules from Different Stages of Lactation: A Lipid Composition Analysis and Microstructure Characterization**, in *Journal of Agricultural and Food Chemistry*. 2012, American Chemical Society. p. 7158-7167.

27. Jensen, R.G., M.M. Hagerty, and K.E. McMahon, **Lipids of human milk and infant formulas: a review**. American Journal of Clinical Nutrition,31 (1978), pp. 990-1016.
28. Jensen, R.G., **Lipids in human milk**, in *Lipids*. 1999. p. 1243-1271.
29. Lopez, C. and O. Ménard, **Human milk fat globules: Polar lipid composition and in situ structural investigations revealing the heterogeneous distribution of proteins and the lateral segregation of sphingomyelin in the biological membrane**. Colloids and Surfaces B: Biointerfaces,83 (2011), pp. 29-41.
30. Yehuda, S., S. Rabinovitz, and D. Mostofsky, **Essential fatty acids and the brain: from infancy to aging**, in *Neurobiol Aging*. 2005. p. 98-102.
31. Evers, J.M., et al., **Heterogeneity of milk fat globule membrane structure and composition as observed using fluorescence microscopy techniques**. International Dairy Journal,18 (2008), pp. 1081-1089.
32. Gallier, S., et al., **Using Confocal Laser Scanning Microscopy To Probe the Milk Fat Globule Membrane and Associated Proteins**. Journal of Agricultural and Food Chemistry,58 (2010), pp. 4250-4257.
33. Langmuir, I., **The constitution and fundamentals properties of solids and liquids.II Liquids.** 39 (1917), pp. 1848-1906.
34. Vollhardt, D., **Morphology and phase behavior of monolayers**, in *Advances in Colloid and Interface Science*. 1996. p. 143-171.
35. Gallier, S., et al., **Surface Characterization of Bovine Milk Phospholipid Monolayers by Langmuir Isotherms and Microscopic Techniques**. Journal of Agricultural and Food Chemistry,58 (2010), pp. 12275-12285.
36. Bourlieu, C., et al., **Specificity of infant digestive conditions: some clues for developing relevant in vitro models**, in *Critical Reviews in Food Science and nutrition*. 2014. p. 1427-1457.
37. Moreau, H., et al., **Human preduodenal lipase is entirely of gastric fundic origin**, in *Gastroenterology*. 1988. p. 1221-1226.
38. Sams, L., et al., **Relevant pH and lipase for in vitro models of gastric digestion**. Food & Function,7 (2016), pp. 30-45.
39. Lindquist, S. and O. Hernell, **Lipid digestion and absorption in early life: an update**. Current Opinion in Clinical Nutrition and Metabolic Care,13 (2010), pp. 314-320.
40. Sarles, J., H. Moreau, and R. Verger, **Human gastric lipase: ontogeny and variations in children**. Acta Paediatrica,81 (1992), pp. 511-513.
41. Bernback, S., L. Blackberg, and O. Hernell, **The complete digestion of human milk triacylglycerol in vitro requires gastric lipase, pancreatic colipase-dependent lipase and bile salt stimulated lipase**. Journal of Clinical Investigation,85 (1990), pp. 1221-1225.
42. Bénarouche, A., et al., *Studying gastric lipase adsorption onto phospholipid monolayers by surface tensiometry, ellipsometry and atomic force microscopy*, in *Methods in Enzymology. Volume 583. Enzymology at the membrane Interface: Interfacial enzymology and protein-membrane binding*, M.H.Gelb, Editor. 2017, Academic Press: London. p. 255-276.
43. Bourlieu, C., et al., **Mechanism of adsorption of gastric lipase in model membranes of milk fat globules.**, in *Colloids and Surfaces B-Biointerfaces*. 2016. p. 97-106.

44. Roussel, A., et al., **Crystal Structure of Human Gastric Lipase and Model of Lysosomal Acid Lipase, Two Lipolytic Enzymes of Medical Interest**. Journal of Biological Chemistry,274 (1999), pp. 16995-17002.
45. Bénarouche, A., et al., **New insights into the pH-dependent interfacial adsorption of dog gastric lipase using the monolayer technique**. Colloids and Surfaces B: Biointerfaces,111 (2013), pp. 306-312.
46. Bourlieu, C., et al., **Hydrolysis of native milk fat globules by microbial lipases: Mechanisms and modulation of interfacial quality**. Food Research International,40 (2012), pp. 533-544.
47. Berge, B. and A. Renault, **Ellipsometry Study of 2D Crystallization of 1-Alcohol Monolayers at the Water Surface**. Europhysics Letters (EPL),21 (1993), pp. 773-777.
48. Smaby, J.M., et al., **Phosphatidylcholine acyl unsaturation modulates the decrease in interfacial elasticity induced by cholesterol**. Biophysical Journal,73 (1997), pp. 1492-1505.
49. Derde, M., et al., **Native lysozyme and dry-heated lysozyme interactions with membrane lipid monolayers: Lateral reorganization of LPS monolayer, model of the Escherichia coli outer membrane**. Biochimica et Biophysica Acta (BBA) - Biomembranes,1848 (2015), pp. 174-183.
50. Pichot, R., R.L. Watson, and I.T. Norton, **Phospholipids at the Interface: Current Trends and Challenges**. Int J Mol Sci,14 (2013), pp. 11767-11794.
51. Petelska, A.D., M. Naumowicz, and Z.A. Figaszewski, **Influence of pH on Sphingomyelin Monolayer at Air/Aqueous Solution Interface**. Langmuir,28 (2012), pp. 13331-13335.
52. Vié, V., et al., **Distribution of Ganglioside GM1 between Two-Component, Two-Phase Phosphatidylcholine Monolayers**, in *Langmuir*. 1998, American Chemical Society. p. 4574-4583.
53. Garcia-Saez, A.J., S. Chiantia, and P. Schwille, **Effect of Line Tension on the Lateral Organization of Lipid Membranes**. Journal of Biological Chemistry,282 (2007), pp. 33537-33544.
54. Saccani, J., et al., **A phospholipid bilayer supported under a polymerized Langmuir film**. Biophysical journal,85 (2003), pp. 3781-3787.
55. Jacquemet, A.T., N.; Benvegnu, T; Vié, V.; Lemiègre, L, **Collapsed bipolar glycolipids at the air/water interface: Effect of the stereochemistry on the stretched/bent conformations**. Journal of Colloid and Interface Science,412 (2013), pp. 72-81.
56. McMahon, H.T. and E. Boucrot, **Membrane curvature at a glance**. Journal of Cell Science,128 (2015), pp. 1065.
57. Danthine, S. and C. Blecker, **Interactions of lipases with milk fat globule membrane monolayers using a Langmuir film balance**. International Dairy Journal,35 (2014), pp. 81-87.
58. Onuki, Y., et al., **Docosahexaenoic Acid and Eicosapentaenoic Acid Induce Changes in the Physical Properties of a Lipid Bilayer Model Membrane**. Chemical and Pharmaceutical Bulletin,54 (2006), pp. 68-71.
59. Stillwell, W. and S.R. Wassall, **Docosahexaenoic acid: membrane properties of a unique fatty acid**. Chemistry and Physics of Lipids,126 (2003), pp. 1-27.
60. Dumaual, A.C., L.J. Jenski, and W. Stillwell, **Liquid crystalline/gel state phase separation in docosahexaenoic acid-containing bilayers and monolayers**. Biochimica et Biophysica Acta (BBA) - Biomembranes,1463 (2000), pp. 395-406.

61. Mitchell, D.C., Litman, B.J., *Modulation of receptor signaling by phospholipid acyl chain composition*, in *Physiological and Behavioral Functions*, D. Mostofsky, Yehuda, S., Salem Jr., N. , Editor. 2001, Humana Press Inc.: Totowa, NJ. p. 23–40.
62. Contarini, G. and M. Povolo, **Phospholipids in Milk Fat: Composition, Biological and Technological Significance, and Analytical Strategies**, in *Int. J. Mol. Sci*. 2013. p. 2808-2831.
63. Roussel, A., et al., **Crystal Structure of the Open Form of Dog Gastric Lipase in Complex with a Phosphonate Inhibitor**. Journal of Biological Chemistry,277 (2002), pp. 2266-2274.
64. López-Montero, I., M. Vélez, and P.F. Devaux, **Surface tension induced by sphingomyelin to ceramide conversion in lipid membranes**. Biochimica et Biophysica Acta (BBA) - Biomembranes,1768 (2007), pp. 553-561.
65. Balashev, K., et al., **Novel methods for studying lipids and lipases and their mutual interaction at interfaces. Part I. Atomic force microscopy**. Biochimie,83 (2001), pp. 387-397.
66. Balashev, K., et al., **Atomic force microscope visualization of lipid bilayer degradation due to action of phospholipase A2 and Humicola lanuginosa lipase**. Biochimica et Biophysica Acta (BBA) - Biomembranes,1768 (2007), pp. 90-99.
67. Nielsen, L.K., et al., **Lag-burst kinetics in phospholipase A2 hydrolysis of DPPC bilayers visualized by atomic force microscopy**. Biochimica et Biophysica Acta (BBA) - Biomembranes,1420 (1999), pp. 266-271.
68. Prim, N., et al., **Atomic force microscope studies on the interactions of Candida rugosa lipase and supported lipidic bilayers**. Colloids and Surfaces B: Biointerfaces,52 (2006), pp. 138-142.
69. Chu, B.S., et al., **Adsorption of Bile Salts and Pancreatic Colipase and Lipase onto Digalactosyldiacylglycerol and Dipalmitoylphosphatidylcholine Monolayers**, in *Langmuir*. 2010, American Chemical Society. p. 9782-9793.
70. Andersson, E., et al., **Bile salt-stimulated lipase and pancreatic lipase related protein 2 promote efficient lipid digestion and product absorption in the newborn**, in *Journal of Pediatric Gastroenterology and Nutrition*. 2011. p. E87-E88.
71. Sodhi, C.P., et al., **Fat composition in infant for u a contributes to the severity of necrotising enterocolitis**. British Journal of Nutrition,120 (2018), pp. 665-680.

Figure legends

Figure 1: Milk fat globule biological secretion and complex structure. Adapted with modifications from [1, 3, 13].

Figure 2: Compression isotherms of HMM (blue) and BMM (grey) extracts. (A) the graph corresponds to the surface pressure versus the area per mg. (B) the graph presents the ellipsometric angle evolution when the surface pressure increases. Surface compressibility moduli (C_s^{-1}) of HMM (C) and BMM extracts (D) calculated following equation 1. The experiments were performed using sodium acetate buffer at pH 5 and were done in duplicate.

Figure 3: Brewster angle microscopy of HMM and BMM extracts upon increasing surface pressure. The image size is 450 × 390 µm² surface. The experiments were performed using

sodium acetate buffer at pH 5 and done in duplicate.

Figure 4: AFM topographic images of the HMM interfacial film transferred at different surface pressure along the isotherm and using the Langmuir-Blodgett method. Each sample corresponds at one experiment. They were performed using sodium acetate buffer at pH 5 and done in triplicate.

Figure 5: AFM topographic images of the BMM interfacial film transferred at different surface pressure along the isotherm and using the Langmuir-Blodgett method. Each sample corresponds at one experiment. They were performed using sodium acetate buffer at pH 5 and done in triplicate.

Figure 6: AFM topographic images of Langmuir-Blodgett monolayers of HMM and BMM extracts before and after rDGL injection (end of the adsorption kinetic). The initial lipid surface pressure was 20mN/m. The image size are 20×20µm², 8×8 µm² in absence (-rDGL) or in presence (+rDGL) of rDGL. Images of the top correspond to the HMM extract while these below correspond to the BMM extract. Right panel, representative cross-section of sample in the presence of rDGL used to determine the average differences of height between LC and LE phases which are summarized in Table 2.

Figure 7: Langmuir-Schaefer transfer of rDGL/lipid monolayer onto hydrophobic mica support and liquid cell AFM imaging. The experiments were performed using sodium acetate buffer at pH 5.

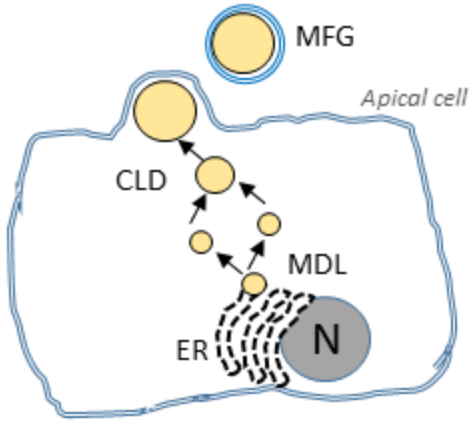

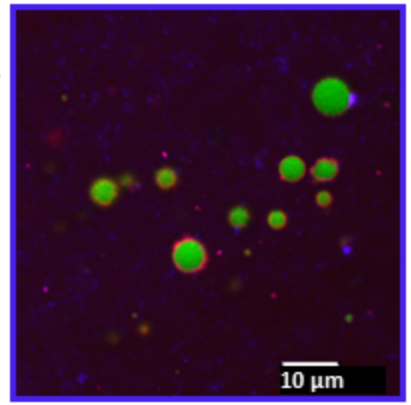

Lipid droplets are formed in the endoplasmic reticulum (ER) by budding into the cytosolic compartment as very small droplets called microlipid droplets (MLD). Droplets increase in size by fusing, giving birth to larger droplets called cytoplasmic lipid droplets (CLD). At the apical cell surface droplets are secreted by envelopment in apical plasma membrane, releasing the milk lipid globule (MLG)

MILK FAT GLOBULES

(average diameter 4 µm, range 0.1-10 µm)

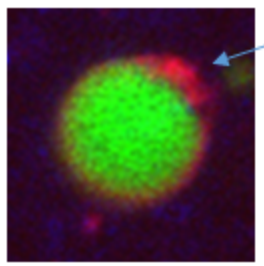

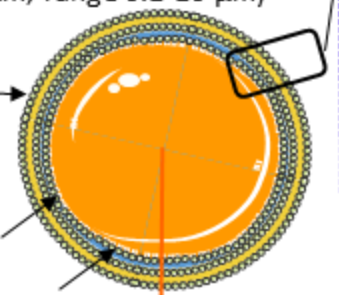

Bilayer (from from the apical plasma membrane of the mammary epithelial cells)

Primary membrane

Cytoplasmic crescent from mammary cell (with enclosed RNA and miRNA)

TAG CORE

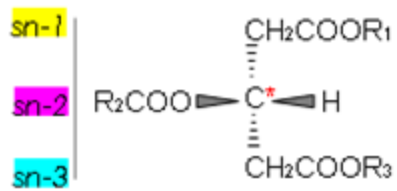

MILK FAT GLOBULES TRILAYERED MEMBRANE

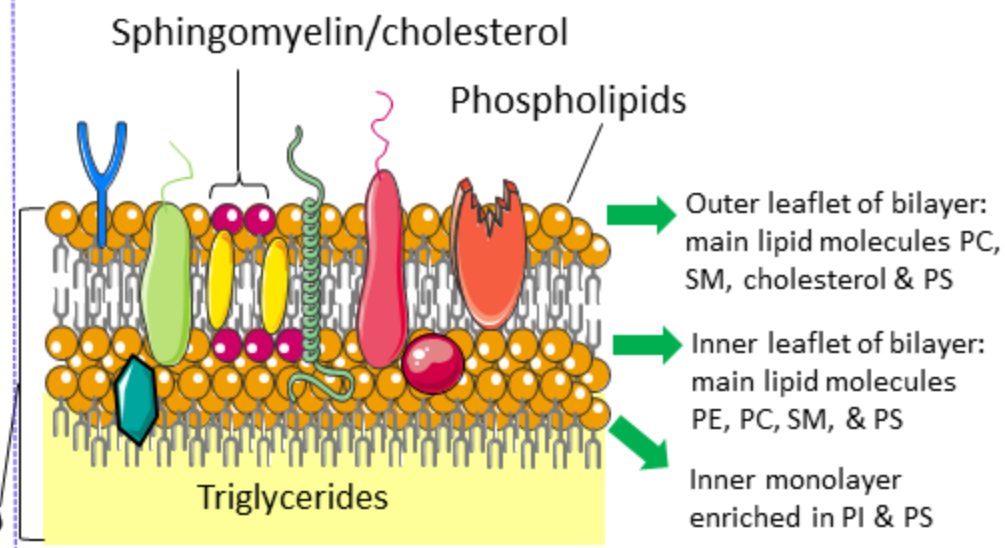

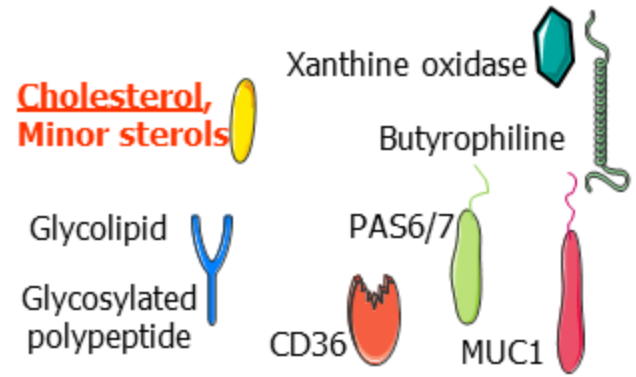

Phospholipid abbreviations: PC phosphatidylcholine, SM sphingomyelin, PE phosphatidylethanolamine, PI phosphatidylinositol, PS Phosphatidylserine.

A)

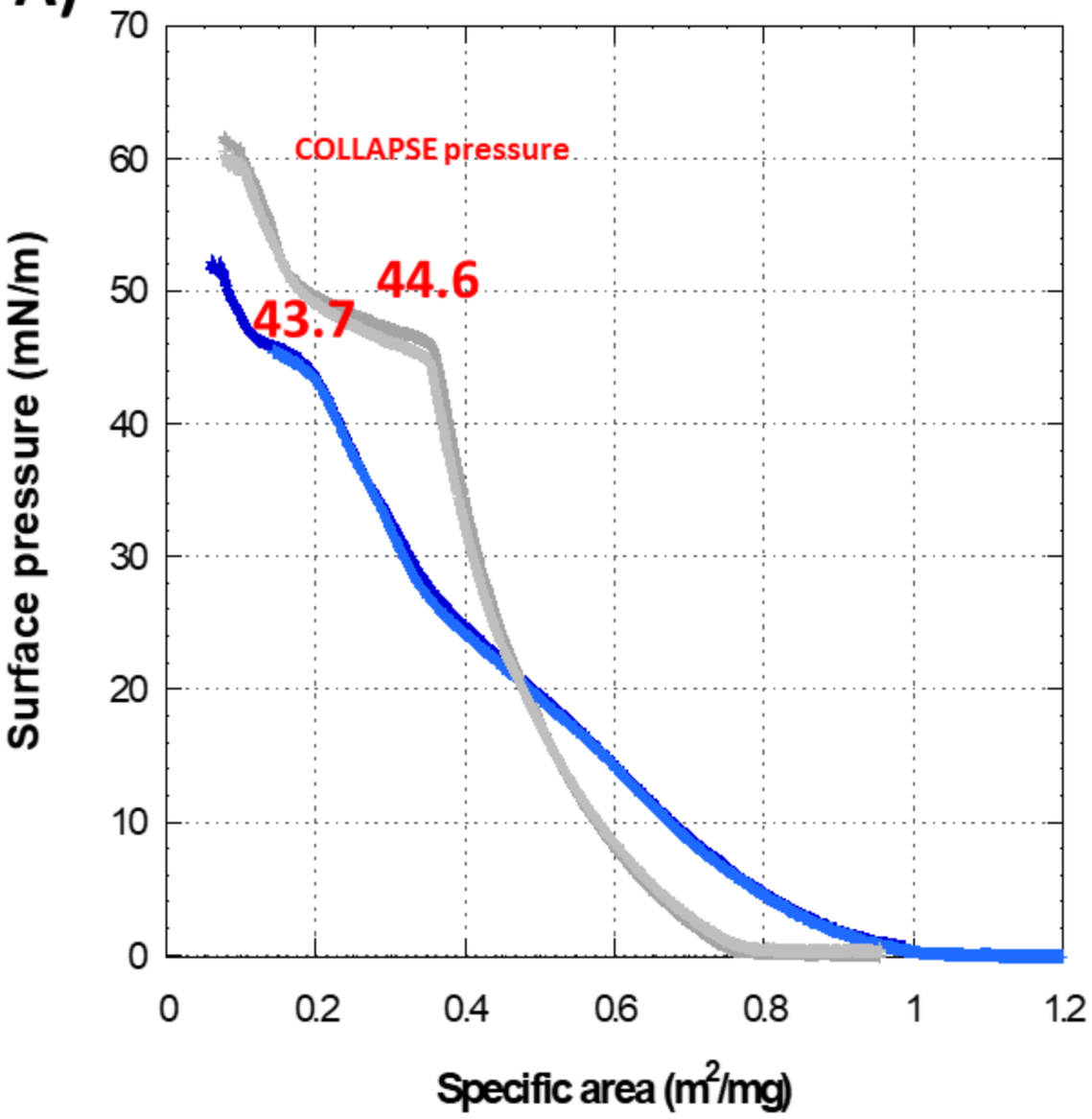
COLLAPSE pressure
44.6
43.7
Surface pressure (mN/m)
Specific area (m²/mg)

B)

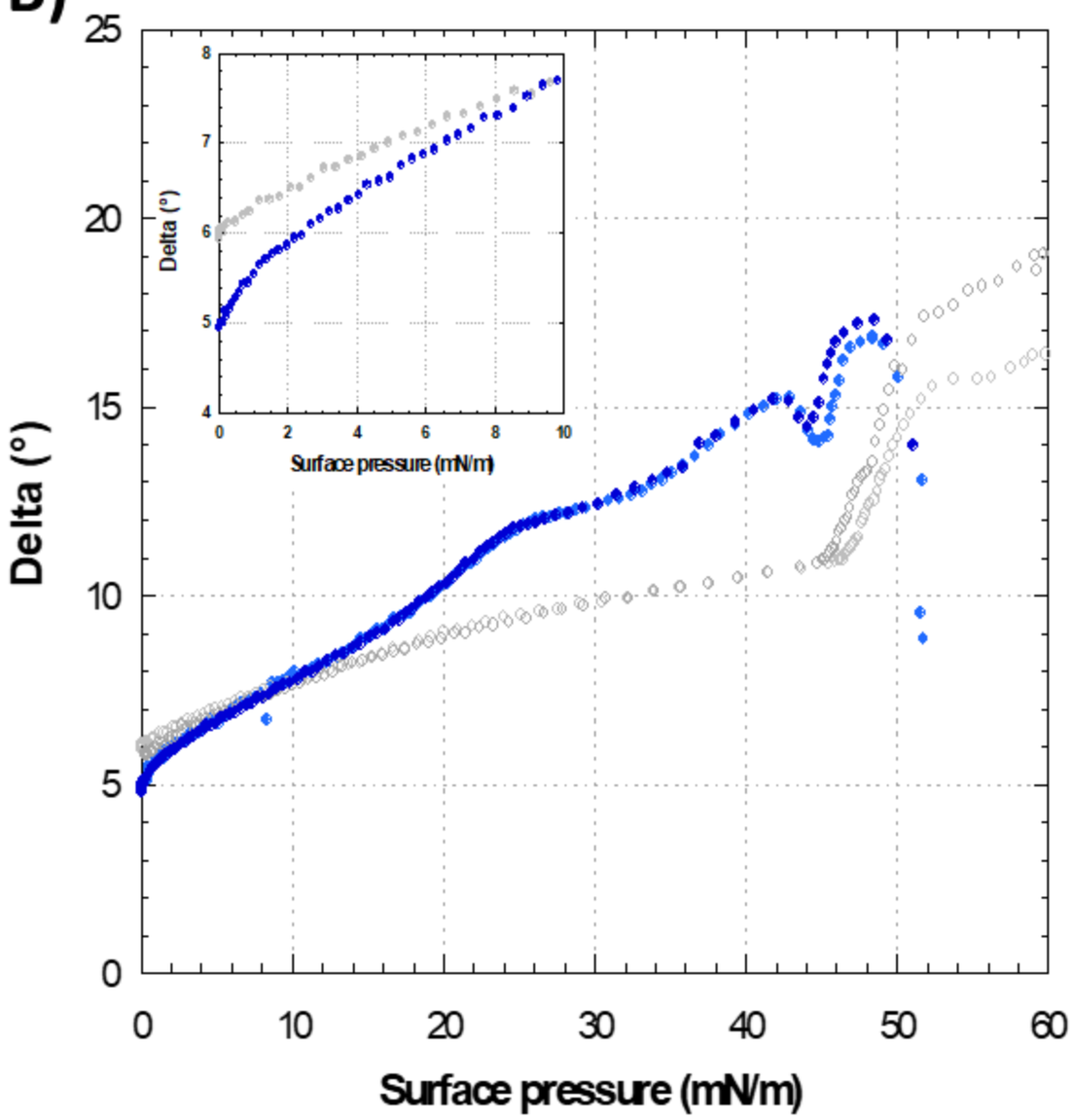
Delta (°)
Surface pressure (mN/m)
Delta (°)
Surface pressure (mN/m)

C)

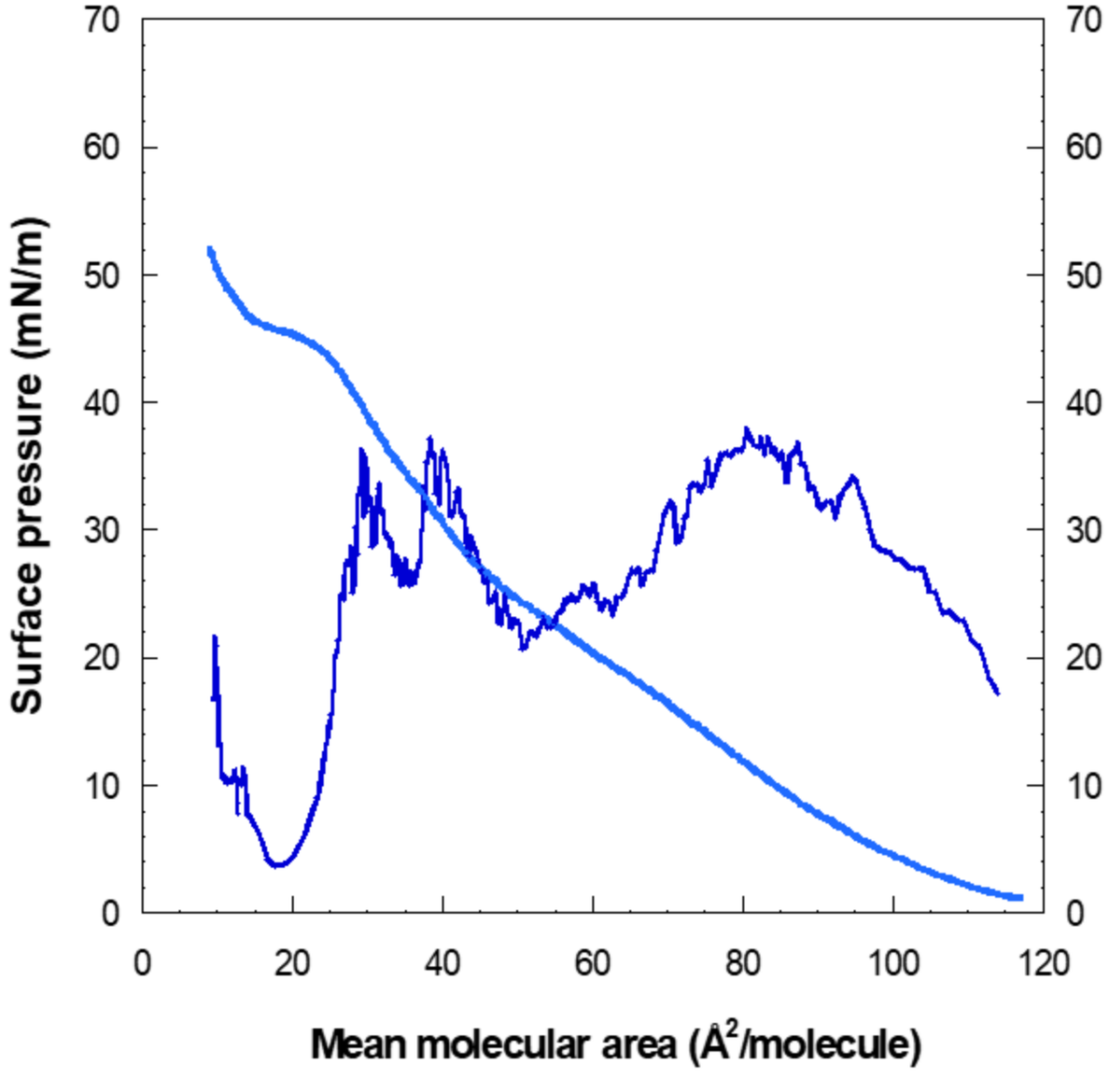
Surface pressure (mN/m)
C_s^-1 (mN/m)
Mean molecular area (Å²/molecule)

D)

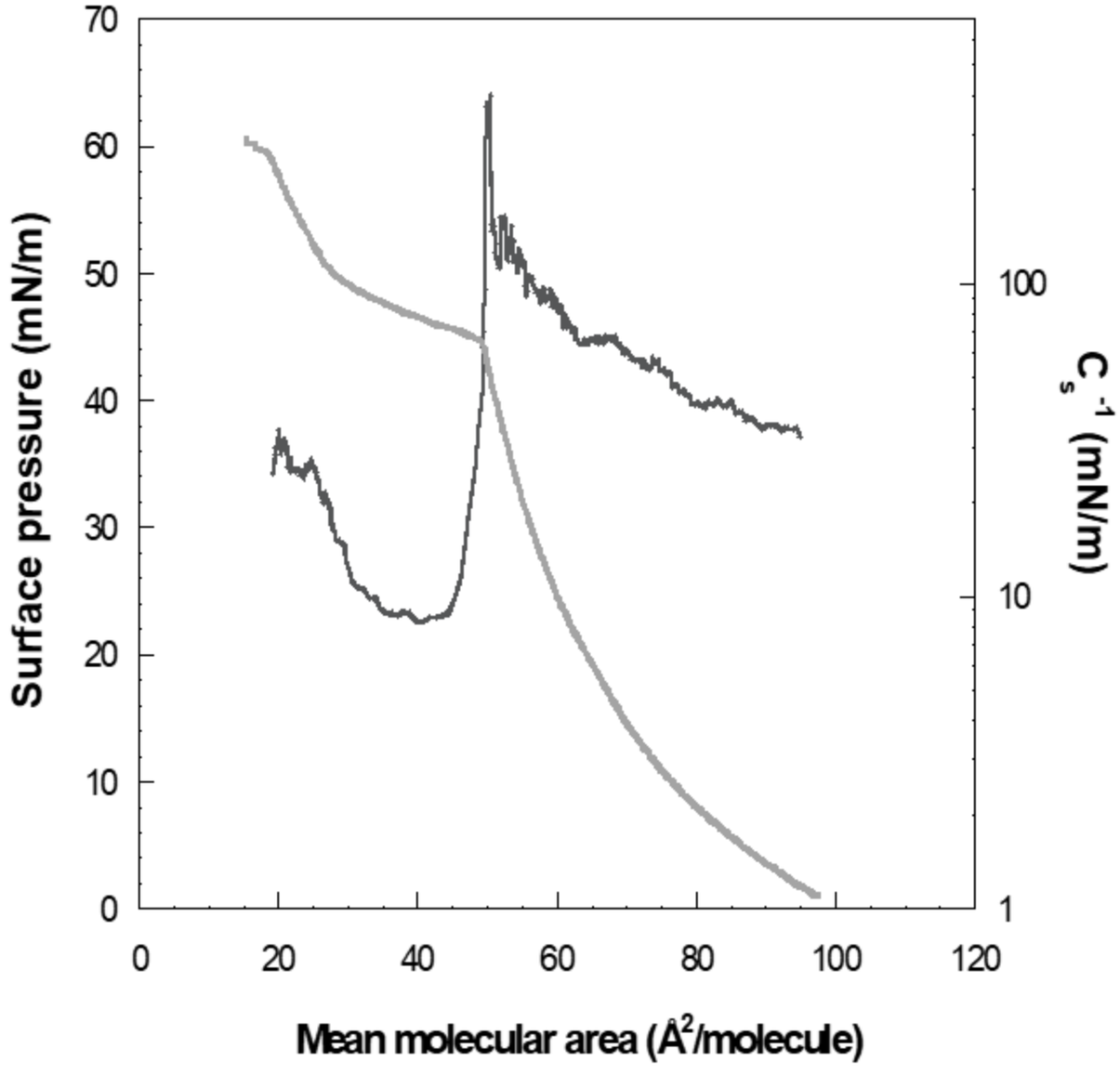
Surface pressure (mN/m)
C_s^-1 (mN/m)
Mean molecular area (Å²/molecule)

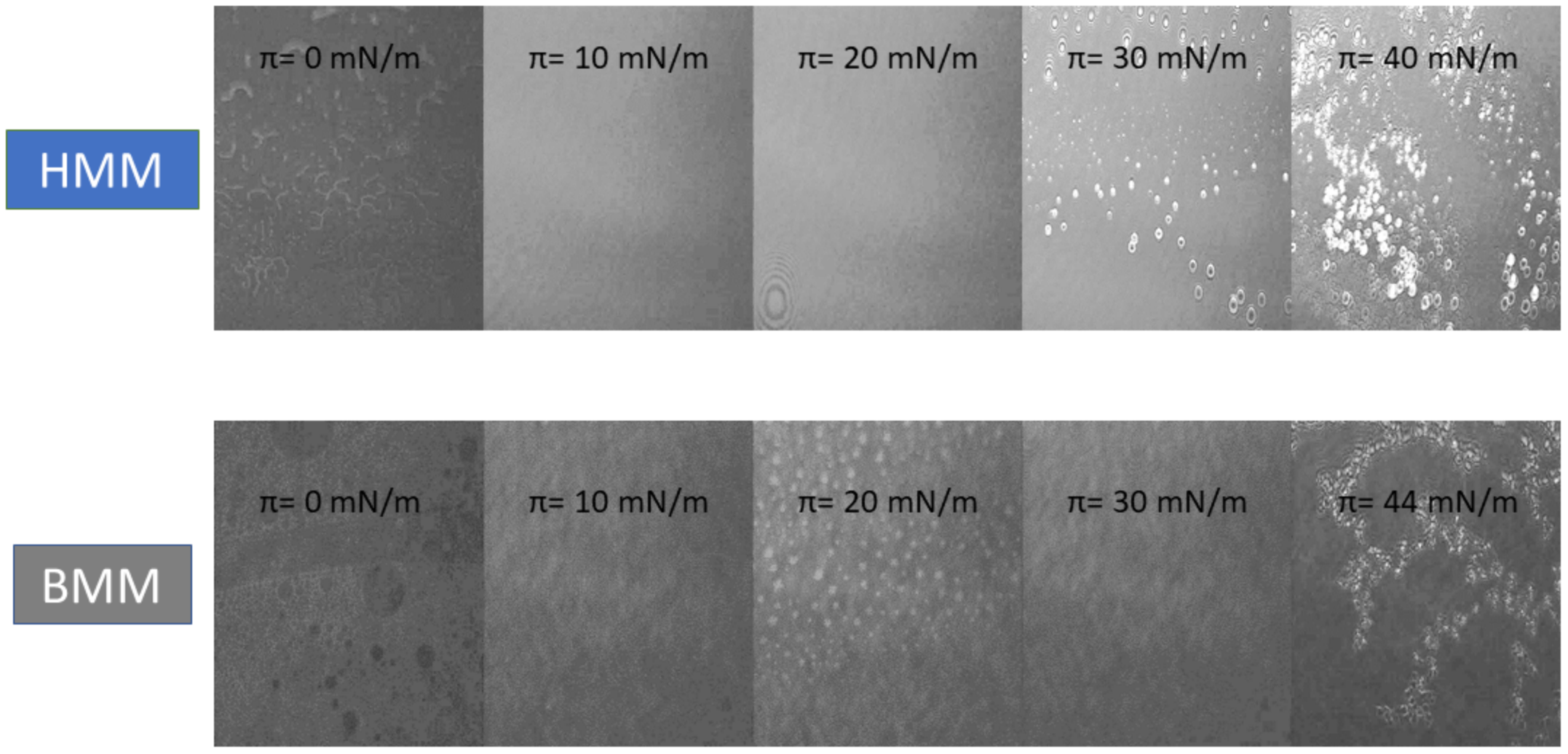
HMM
π= 0 mN/m
π= 10 mN/m
π= 20 mN/m
π= 30 mN/m
π= 40 mN/m
BMM
π= 0 mN/m
π= 10 mN/m
π= 20 mN/m
π= 30 mN/m
π= 44 mN/m

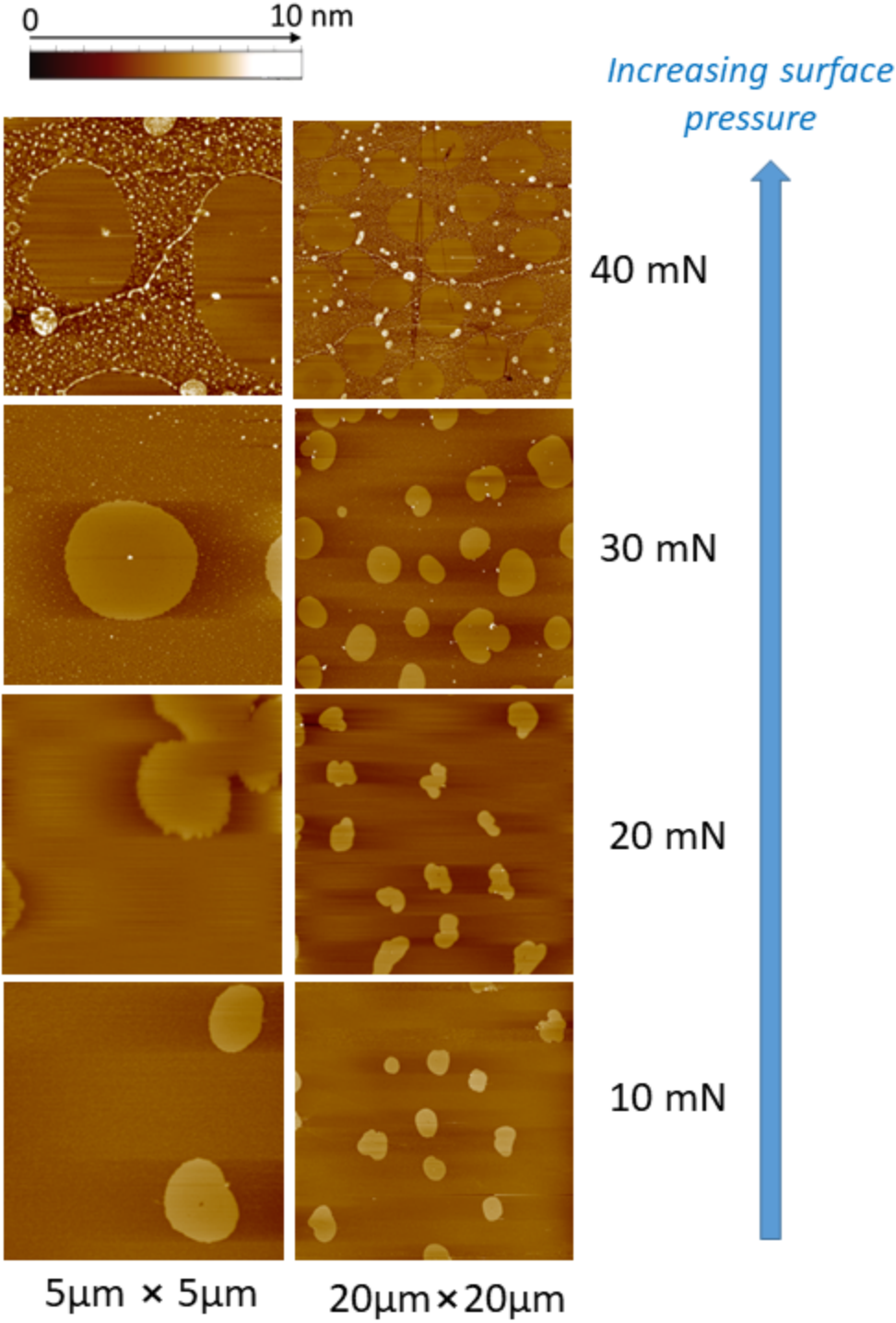
0
10 nm
Increasing surface pressure
40 mN
30 mN
20 mN
10 mN
5μm × 5μm
20μm×20μm

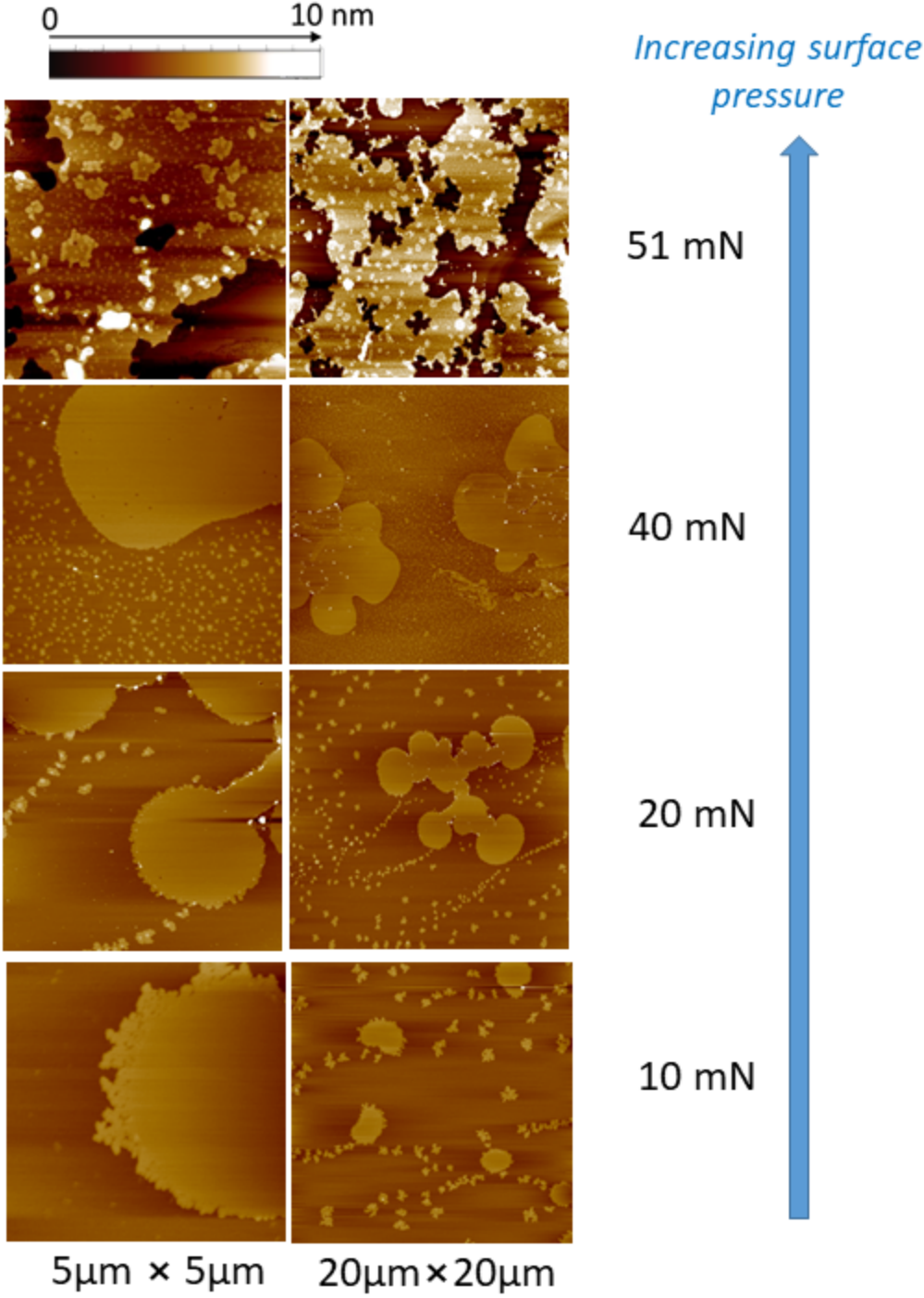
0
10 nm
Increasing surface pressure
51 mN
40 mN
20 mN
10 mN
5µm × 5µm
20µm×20µm

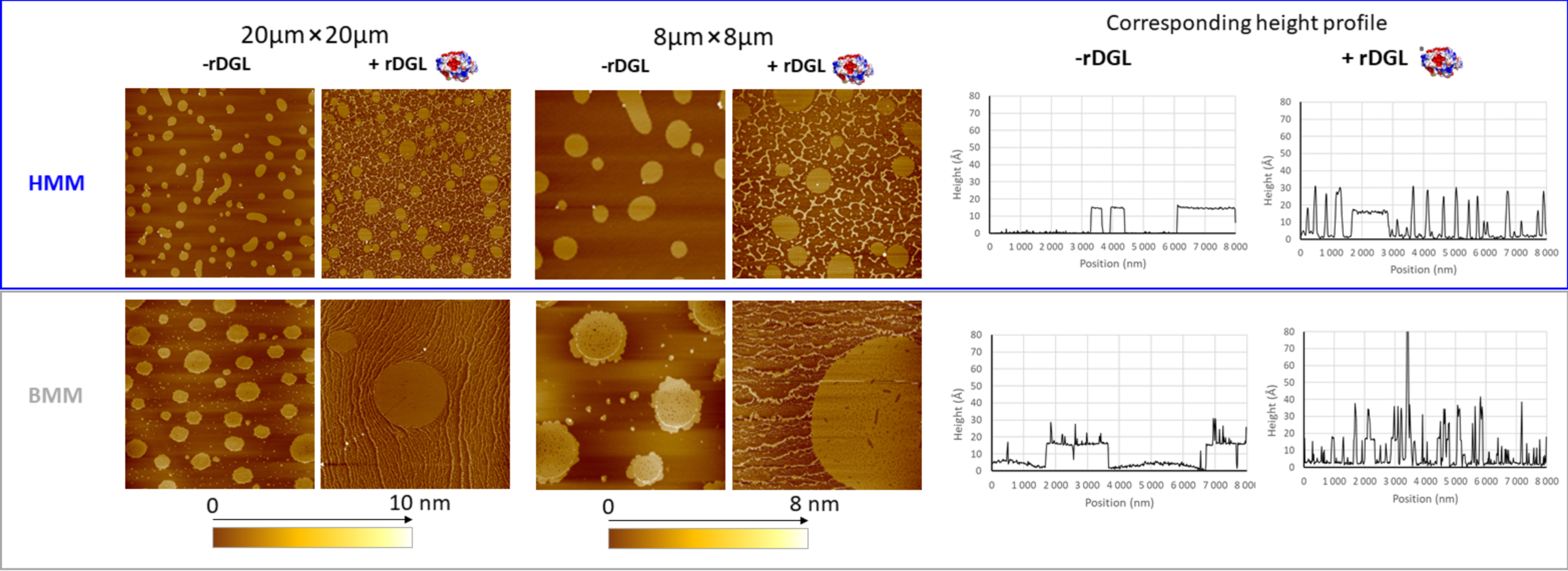
20μm×20μm
-rDGL
+ rDGL
8μm×8μm
-rDGL
+ rDGL
Corresponding height profile
-rDGL
+ rDGL
HMM
BMM
0
10 nm
0
8 nm
Height (Å)
Position (nm)

HMM + rDGL

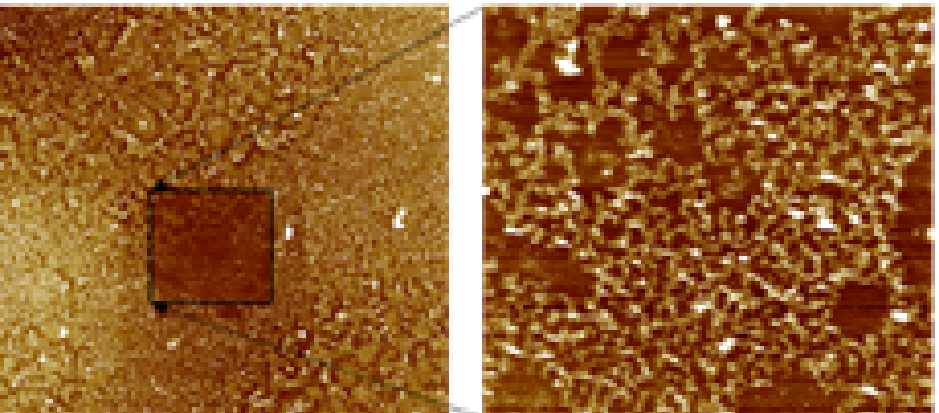

20µm*20µm, Δz=70nm

5µm*5µm, Δz=25nm

BMM + rDGL

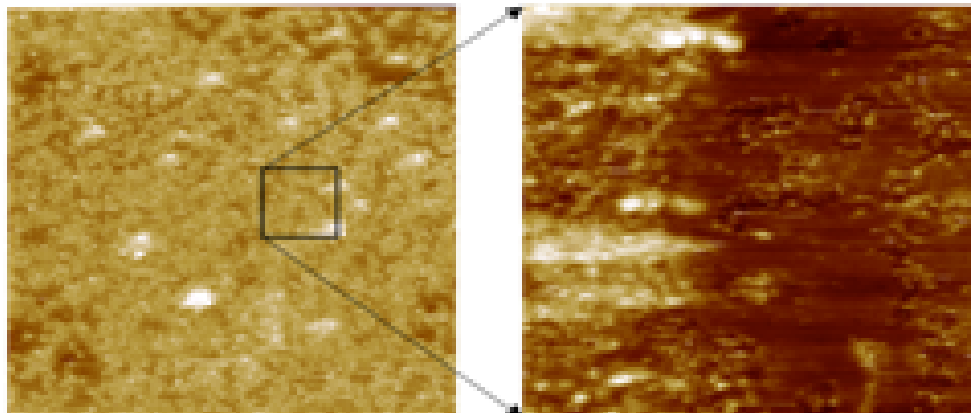

5µm*5µm, Δz=40nm

1µm*1µm, Δz=10nm

Tables

Table 1. Comparison of the chemical composition of human milk membrane (HMM) *versus* bovine milk membrane (BMM) in terms of lipid polar classes and total fatty acids. Average ± standard deviation. T-test: * stands for significant difference using Student test with $p < 0.05$, ** stands for $p < 0.01$. Acyl chains displayed in Table if present at ≥ 0.1 % in at least one of the two extracts.

Abbreviations: PE: Phosphatidylethanolamine; PI: phosphatidylinositol; PS: Phosphatidylserine; PC: Phosphatidylcholine; SM: sphingomyeline; SC: short chains; MC: medium chains; LC: long chains; VLC: very long chains; SFA: saturated fatty acids; USFA: unsaturated fatty acids.

Polar lipids	HMM	BMM	T-test
PE	10,6 ± 1,1	18,9 ± 1,0	**
PI	11,1 ± 0,5	6,6 ± 0,2	*
PS	12,8 ± 0,6	4,1 ± 0,8	**
PC	28,2 ± 0,4	36,1 ± 0,1	**
SM	37,3 ± 2,6	34,2 ± 0,7	
Total PL	**71,4 ± 2,8**	**69,4 ± 3,3**	
Acyl chains			
C4:0	0,0 ± 0,0	0,2 ± 0,0	**
C10:0	0,4 ± 0,0	0,5 ± 0,0	
C12:0	0,8 ± 0,9	0,6 ± 0,0	
C13:0	0,2 ± 0,0	0,0 ± 0,0	**
C14:0	3,0 ± 0,0	5,0 ± 0,0	**
C14:1c9	0,2 ± 0,1	0,1 ± 0,0	
C15:0	0,4 ± 0,0	0,9 ± 0,0	**
C15:1c10	0,1 ± 0,0	0,3 ± 0,0	
C16:0	15,5 ± 0,1	25,5 ± 0,0	**
C16:1c9	2,0 ± 0,0	1,4 ± 0,0	**
C17:0	0,4 ± 0,0	0,6 ± 0,0	**
C17:1c10	0,4 ± 0,0	0,3 ± 0,0	*
C18:0	21,2 ± 0,1	18,4 ± 0,1	
C18:1t10	0,7 ± 0,1	0,7 ± 0,0	
C18:1t11	0,0 ± 0,0	0,5 ± 0,0	**
C18:1t6,t9,t12	0,0 ± 0,0	0,6 ± 0,0	**
C18:1c9	31,8 ± 0,2	31,2 ± 0,1	
C18:2t9,t12	0,2 ± 0,0	0,4 ± 0,0	**
C18:2c9,c12	14,1 ± 0,1	7,0 ± 0,0	**
C18:3c9,c12,c15	0,6 ± 0,0	0,6 ± 0,0	
C20:0	0,3 ± 0,1	0,4 ± 0,0	
C20:4c5,c8,c11,c14	1,5 ± 1,3	0,7 ± 0,0	
C20:1c11	0,7 ± 0,0	0,1 ± 0,0	**
C21:0	0,1 ± 0,0	0,2 ± 0,0	**
C20:2c11,c14	0,2 ± 0,0	0,1 ± 0,0	**
C20:3c8,c11,c14	0,8 ± 0,0	1,0 ± 0,0	*
C20:3c11,c14,c17	1,5 ± 0,0	0,9 ± 0,0	*
C22:0	0,3 ± 0,0	0,5 ± 0,0	*
C22:1c13	0,3 ± 0,1	0,1 ± 0,0	*
C20:5c5,c8,c11,c14,c17	0,2 ± 0,1	0,1 ± 0,0	
C23:0	0,2 ± 0,1	0,4 ± 0,0	*
C24:1c15	0,1 ± 0,1	0,1 ± 0,0	
C24:0	0,2 ± 0,0	0,5 ± 0,0	**
C22:5c7,c10,c13,c16,c19=DPA	0,3 ± 0,0	0,1 ± 0,0	**
C22:6c4,c7,c10,c13,c16,c19=DHA	0,8 ± 0,0	0,3 ± 0,3	*
SC (<C9)	**0,0 ± 0,0**	**0,3 ± 0,0**	*
MC(C9-C14)	**4,6 ± 0,2**	**6,2 ± 1,2**	
LC(C14-C20)	**93,0 ± 0,1**	**91,7 ± 3,7**	
VLC (>C20)	**2,3 ± 0,0**	**2,3 ± 0,2**	
SFA	**42,9 ± 0,1**	**53,8 ± 3,4**	*
USFA	**57,1 ± 0,1**	**46,8 ± 0,0**	*

Table 2. Summary of the various parameters obtained from AFM images analysis using FIJI with (+ rDGL) or without (- rDGL) lipase injected in the subphase.

	- rDGL				**+ rDGL[c]**						
	Average $\Delta_{LC\text{-}LEa}$ (nm)	Area covered by LC (%)	LC Average domain average Area (μm^2)	Circ[b]	Average Δ_{LC-LE} (nm)	Area covered by LC (%)	LC domain average Area (μm^2)	Circ[b]	Small grains		
									Area (%)	Average Area (μm^2)	Circ[b]
BMM	1.5±0.1	27.1	3.2 0.02	0.76 0.96	1.5±0.1	17.7	0.05	0.33	2.9	5.2×10^{-4}	0.97
HMM	1.5±0.1	13.6	0.8	0.80	1.4±0.2	15.8	0.86	0.80	26.1	0.02	0.89

[a]*Values were estimated by 20 random measurements on one image. ± values stand for calculated standard deviation on the 20 measurements.*

[b]*Circularity (Circ) = 4π (particle_area/perimeter^2). A value of 1.0 indicates a perfect circle.*

[c]*In the presence of rDGL, very large microdomains in BMM were excluded from the portion of the analyzed image to get rid of the bias they would trigger on image analysis.*

Human milk membrane isotherm

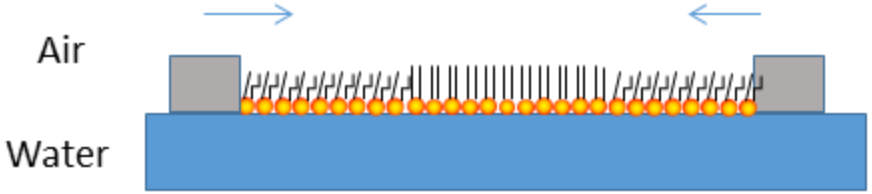

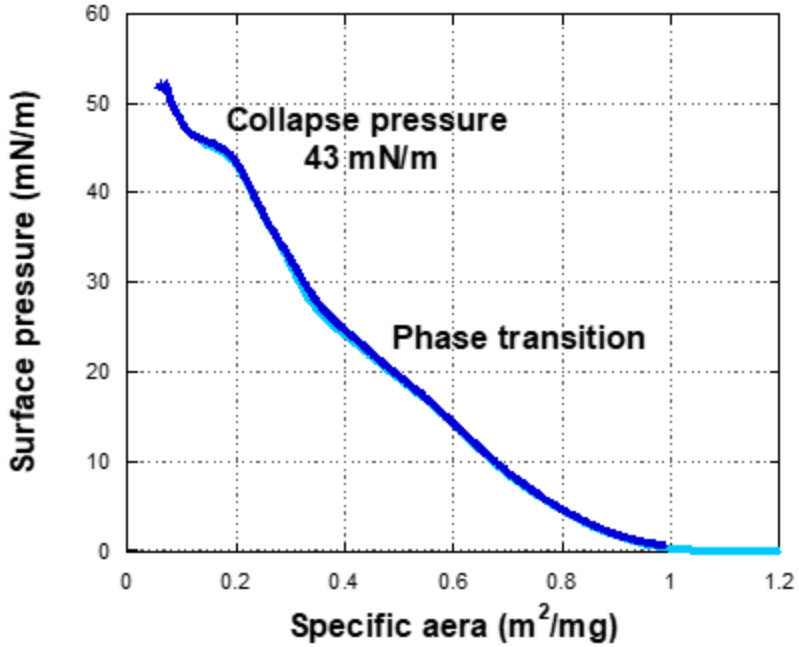

AFM visualisation of rGDL repartition on the human milk membrane

Langmuir-Blodgett transfert

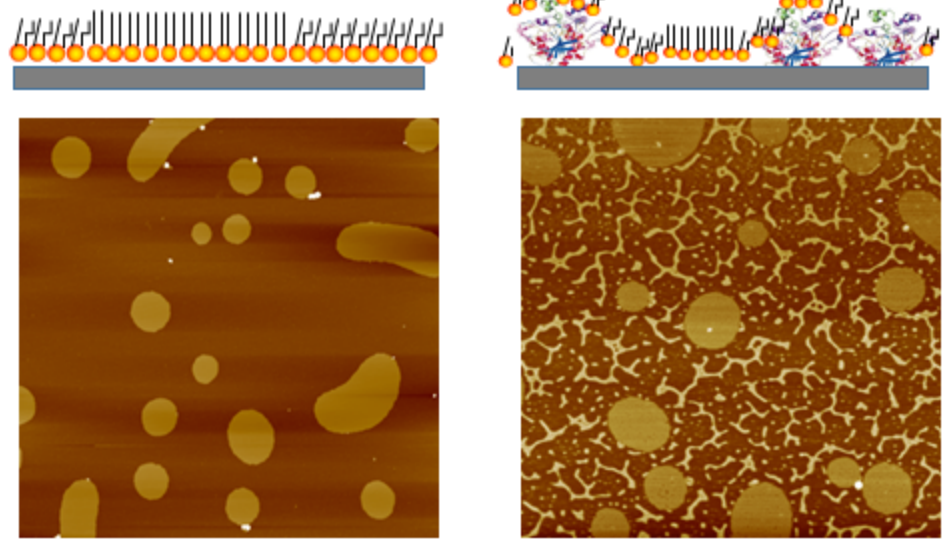

5µm*5µm; Δz=10nm

Langmuir-Schaefer transfert

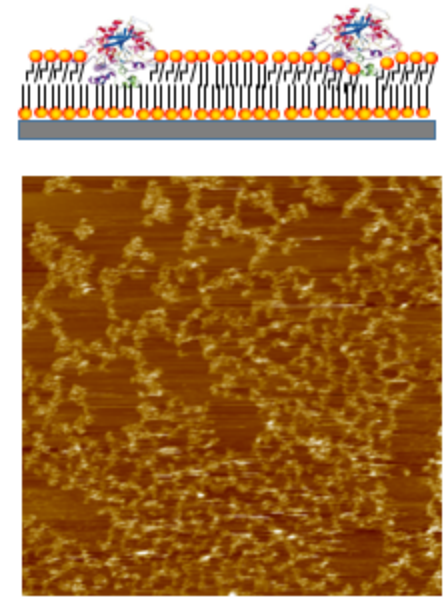

5µm*5µm; Δz=40nm